BIOCHEMISTRY
including biophysical chemistry & molecular biology
Current Topic

DOI:10.1021/bi9002698

Porosome: The Secretory Portal in Cells[†]

Bhanu P. Jena*

Department of Physiology, Wayne State University School of Medicine, Detroit, Michigan 48201

Received February 17, 2009; Revised Manuscript Received April 10, 2009

ABSTRACT: Porosomes are supramolecular, cup-shaped lipoprotein structures at the cell plasma membrane, where membrane-bound secretory vesicles dock and fuse to release intravesicular contents to the outside during cell secretion. The porosome opening to the outside ranges from 150 nm in diameter in acinar cells of the exocrine pancreas to 12 nm in neurons. In the past decade, the composition of the porosome, its structure and dynamics at nanometer resolution in real time, and its functional reconstitution into an artificial lipid membrane have been described. Discovery of the universal secretory machinery in cells, the porosome, came as no surprise since porosome-like "canaliculi" structures for secretion from human platelets, the secretory machinery in single-cell organisms like the secretion apparatus in bacteria and *Toxoplasma gondii*, and the contractile vacuole in paramecium have been demonstrated. In this review, the discovery of the porosome complex and the molecular mechanism of its function and how this information provides a new understanding of cell secretion are discussed.

All life processes are governed at the chemical level, and therefore, knowledge of how single molecules are arranged and interact provides a fundamental understanding of Nature. An aspect of molecular interactions is the assembly of supramolecular structures for the purpose of performing specific cellular functions. Secretion, for example, is a fundamental cellular process responsible for numerous physiological activities in living organisms, such as neurotransmission and the release of hormones and digestive enzymes. Secretory defects in cells are responsible for a host of debilitating diseases, and hence, this field has been the subject of intense study for more than half a century. Only in the past decade using atomic force microscopy (AFM)[1] have discovery of the "porosome", a supramolecular structure at the cell plasma membrane measuring only a few nanometers, and its determination as the universal secretory machinery in cells finally provided a molecular understanding of cell secretion. In cells, secretory products packed and stored in membranous sacs or vesicles dock and establish continuity at the base of plasma membrane-associated structures called porosomes (Figure 1) (*1*−*9*), to release their contents to the outside. The subsequent isolation of the porosome and the determination of its biochemical composition, its structure and dynamics at nanometer resolution and in real time, and its functional reconstitution into an artificial lipid membrane (*1*−*9*) have greatly advanced our understanding of the secretory process in cells, echoed by a number of investigators (*10*−*32*). It is fascinating how even single-cell organisms have developed such specialized secretory machinery, like the secretion apparatus of *Toxoplasma gondii* (Figure 1F) (*33*), the contractile vacuole in paramecium (*34*), and the secretory structures in bacteria (*35*). Hence, it comes as no surprise that mammalian cells have evolved such highly specialized and sophisticated cup-shaped structures, the porosome complex, or the porosome-like "canalicular systems" in human platelets (Figure 1E) (*36*, *37*), for the precise and regulated expulsion of intravesicular contents from cells, from neurotransmission, to the secretion of hormones from endocrine cells, and digestive enzymes from the exocrine pancreas. In every case, secretory vesicles have a much larger surface area, several-fold larger than that of the porosome complex. During cell secretion, the porosome opening dilates to enable release of sectory products, returning to its resting size following completion of secretion. According to conventional belief, if secretory vesicles were to completely merge at the porosome, it would result in a total obliteration of the porosome complex, since the surface areas of secretory vesicles are several-fold larger than that of the porosome. Studies discussed in this review demonstrate that secretory vesicles transiently dock and fuse at the base of porosomes to expel intravesicular contents during cell secretion (Figure 2). This mechanism is in contrast to the general belief that in mammalian cells, secretory vesicles completely merge at the cell plasma membrane, resulting in passive diffusion of vesicular contents to the cell exterior. Furthermore, a major logistical problem with complete merging of the secretory vesicle membrane at the cell plasma membrane is the presence of partially empty vesicles following cell secretion.

[†]This work was supported by grants from NSF (CBET-0730768) and NIH (NS-39918) and a Wayne State University Research Enhancement Award (B.P.J.).

*To whom correspondence should be addressed: Department of Physiology, Wayne State University School of Medicine, 5245 Scott Hall, Detroit, MI 48201. Phone: (313) 577-1532. Fax: (313) 993-4177. E-mail: bjena@med.wayne.edu.

[1]Abbreviations: SNARE, *N*-ethylmaleimide-sensitive factor; NSF, attachment protein receptors; t-SNAREs, target SNAREs; v-SNARE, vesicle SNARE or VAMP or vesicle-associated membrane protein; AFM, atomic force microscopy; CD, circular dichroism; ZG, zymogen granule; GH, growth hormone.

Published on Web 4/13/2009

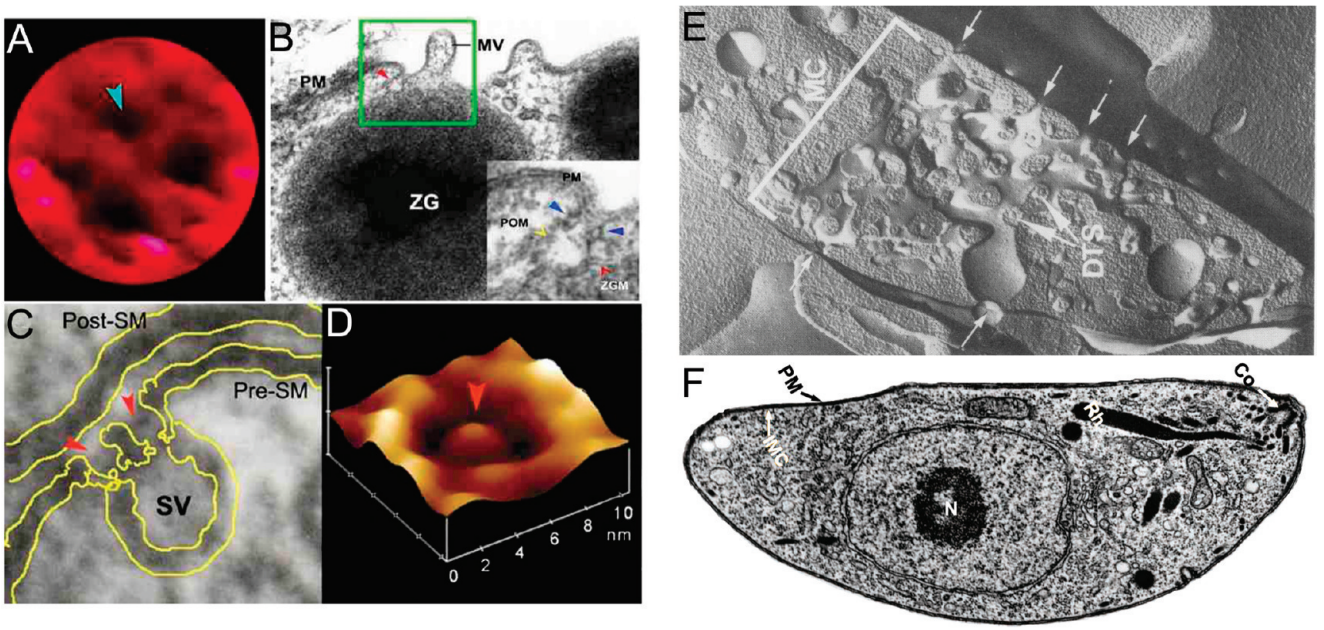

FIGURE 1: Porosomes, previously termed "depressions" at the plasma membrane in pancreatic acinar cells and at the nerve terminal. (A) High-resolution AFM micrograph showing a single pit with four 100−180 nm porosomes within (blue arrowhead) at the apical plasma membrane in a live pancreatic acinar cell. (B) Electron micrograph depicting a porosome (red arrowhead) close to a microvilli (MV) at the apical plasma membrane (PM) of a pancreatic acinar cell. Note the association of the porosome membrane (yellow arrowhead) and the zymogen granule membrane (ZGM) (red arrowhead) of a docked ZG (inset). A cross section of a circular complex at the mouth of the porosome is shown (blue arrowhead). (C) Electron micrograph of a porosome (red arrowhead) at the nerve terminal, in association with a synaptic vesicle (SV) at the presynaptic membrane (Pre-SM). Notice the central pluglike structure at the neuronal porosome opening. (D) AFM micrograph of a neuronal porosome in physiological buffer, also showing the central plug (red arrowhead) at its opening. The central plug in the neuronal porosome complex may regulate its rapid close−open conformation during neurotransmitter release. The neuronal porosome is 1 order of magnitude smaller (10−15 nm) compared to the porosome in the exocrine pancreas (*22*). (E) Electron micrograph of a freeze-fractured discoid platelet. The organization and intercommunication of open calaliculi system (OCS) demonstrating docked and fused secretory vesicles. Several apertures (T) of the OCS open into a communicating web of fenestrated channels that stretches across the cytoplasm to openings (t) at the cell membrane. Elements of the dense tubular system (DTS) are interwoven with channels of the OCS in membrane complexes (MC) within the platelet (27000×). Reprinted with permission from ref *37*. Copyright 1980 American Society for Investigative Pathology. (F) *T. gondii* parasite possessing a stable polarized secretory apparatus and a micropore (right). The secretory apparatus has three morphologically distinct organelles, namely, micronemes, rhoptries (Rh), and dense granules. The conoid (Co) is present at the apical end of the parasite. Note the micropore is continuous with the plasma membrane (PM) of the parasite. The parasite also has an inner membrane complex (IMC). Reprinted with permission from ref *33*. Copyright 2002 Rockefeller University Press.

The establishment of continuity between the secretory vesicle membrane and the porosome membrane requires the participation of specific membrane proteins called SNAREs (*38*−*42*). At the nerve terminal, for example, target membrane proteins SNAP-25 (*38*) and syntaxin (*39*), collectively called t-SNAREs present at the base of the neuronal porosome complex, and synaptic vesicle-associated membrane protein v-SNARE (*40*) are involved in fusion of synaptic vesicles at the porosome base (*41*, *42*). To understand SNARE-induced membrane fusion, a comprehension of the interaction and assembly of membrane-associated v-SNARE and t-SNARE proteins is required. Solubility problems have precluded the generation of three-dimensional (3D) crystals of membrane-associated t-/v-SNARE complexes. However, when the membrane-associated hydrophobic domain of the t-SNARE protein syntaxin and the v-SNARE protein VAMP (vesicle-associated membrane protein) were truncated, the proteins were rendered soluble, allowing 3D crystallization of the truncated t-/v-SNARE complex and the determination of its structure at 2.4 Å (*43*). Unfortunately, it soon became apparent that in the absence of membrane, t-SNAREs and v-SNARE interact differently (*44*), thereby precluding formation of the physiologically relevant t-/v-SNARE complex in cells. The structure and arrangement of the membrane-associated t-/v-SNARE complex were first determined using AFM (*44*). Results from the study demonstrate that t-SNAREs and v-SNARE, when present in opposing bilayers, interact in a circular array to form ring complexes or channels, each measuring a few nanometers (Figure 3) (*44*). The size of the ring complex is directly proportional to the curvature of the opposing bilayers, and in the presence of calcium, the SNARE ring complex enables the establishment of continuity between the opposing bilayers. In contrast, in the absence of membrane association, soluble v- and t-SNAREs fail to assemble in such organized rings or establish continuity between the opposing bilayers (*44*, *45*). Once v-SNARE and t-SNAREs residing in opposing bilayers meet, the resulting SNARE complex overcomes the repulsive forces between opposing bilayers, bringing them within a distance of 2.8−3 Å. This allows calcium bridging of the opposing phospholipid headgroups and leads to local dehydration and membrane fusion (*46*−*48*).

In this review, the discovery of the porosome as the universal secretory machinery or portal in cells, its structure, its dynamics, its isolation, its composition, its functional reconstitution in artificial lipid membrane, and the molecular mechanism of SNARE-induced fusion of secretory vesicle at the porosome base are discussed. This work is primarily focused on the porosome in both slow and fast secretory cells, namely, the acinar cell of the exocrine pancreas and neurons, respectively. Additionally, studies on neuronal SNAREs provide an understanding of the molecular mechanism of SNARE-induced

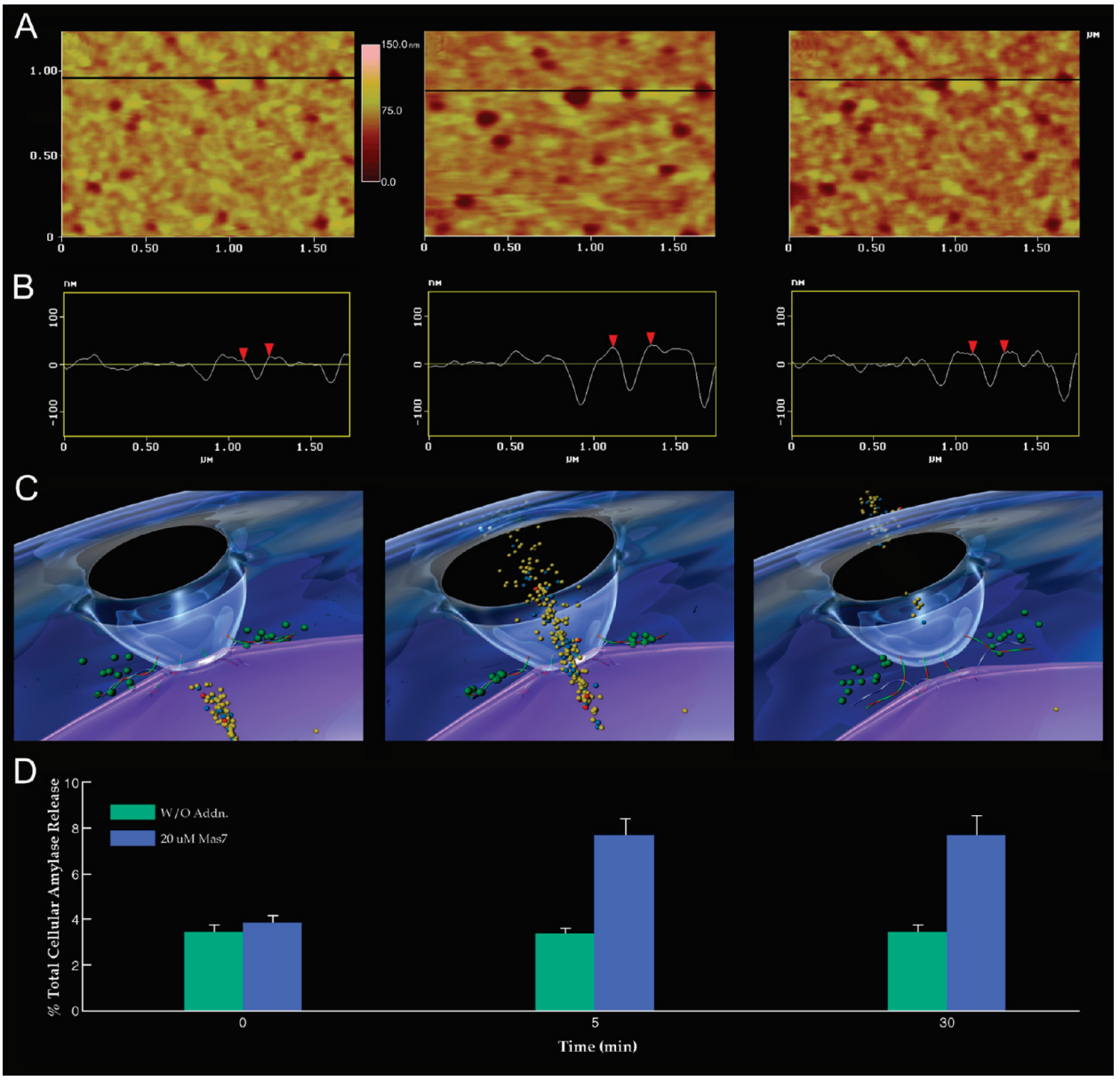

FIGURE 2: Porosome dynamics in pancreatic acinar cells following stimulation of cell secretion. (A) Several porosomes within a pit are shown at time zero and 5 and 30 min following stimulation of secretion. (B) Section analysis across three porosomes in the top panel is represented graphically in the second panel and defines the diameter and relative depth of each of the three porosomes. The porosome at the center is denoted with red arrowheads. (C) The third panel is a three-dimensional rendition of the porosome complex at different times following stimulation of secretion. Note the porosome as a blue cup-shaped structure with a black opening to the outside, and part of a secretory vesicle (violet) docked at its base via t-/v-SNAREs. (D) The bottom panel represents the percent total cellular amylase release in the presence and absence of the secretagogue Mas7 (blue bars). Note an increase in porosome diameter and relative depth, correlating with an increase in the total level of cellular amylase release 5 min following stimulation of secretion. Thirty minutes following a secretory stimulus, there is a decrease in the diameter and relative depth of porosomes and no further increase in amylase release beyond the 5 min time point. No significant changes in amylase secretion (green bars) or porosome diameter were observed in control cells in either the presence or absence of the nonstimulatory mastoparan analogue (Mas17). High-resolution images of porosomes were obtained before and after stimulation with Mas7, for up to 30 min (*1*).

membrane fusion, i.e., the fusion of synaptic vesicles at the porosome base in neurons. The discovery of the porosome complex, and the new insights into its structure−function relationship, have resulted in a paradigm shift in our understanding of cell secretion, which is further discussed in this review.

Discovery of the Porosome, the Universal Secretory Machinery in Cells. Porosomes were first discovered in acinar cells of the exocrine pancreas (*1*). Exocrine pancreatic acinar cells are polarized secretory cells possessing an apical and a basolateral end. This well-characterized cell synthesizes digestive enzymes, which are stored within 0.2−1.2 μm diameter membranous sacs or secretory vesicles called zymogen granules (ZG), located apically. Following a secretory stimulus, ZGs dock and fuse with the apical plasma membrane to release their contents to the outside. In contrast to neurons, in which secretion of neurotransmitters occurs in milliseconds, the pancreatic acinar cells secrete digestive enzymes over minutes following a secretory stimulus. Being slow secretory cells, pancreatic acinar cells were considered ideal for investigating the molecular steps involved in cell secretion. In the mid-1990s, AFM studies on live pancreatic acinar cells were performed to evaluate at high resolution the structure and dynamics of the apical plasma membrane surface, in both resting and stimulated cells. To our surprise, isolated live pancreatic acinar cells in physiological buffer, when imaged using

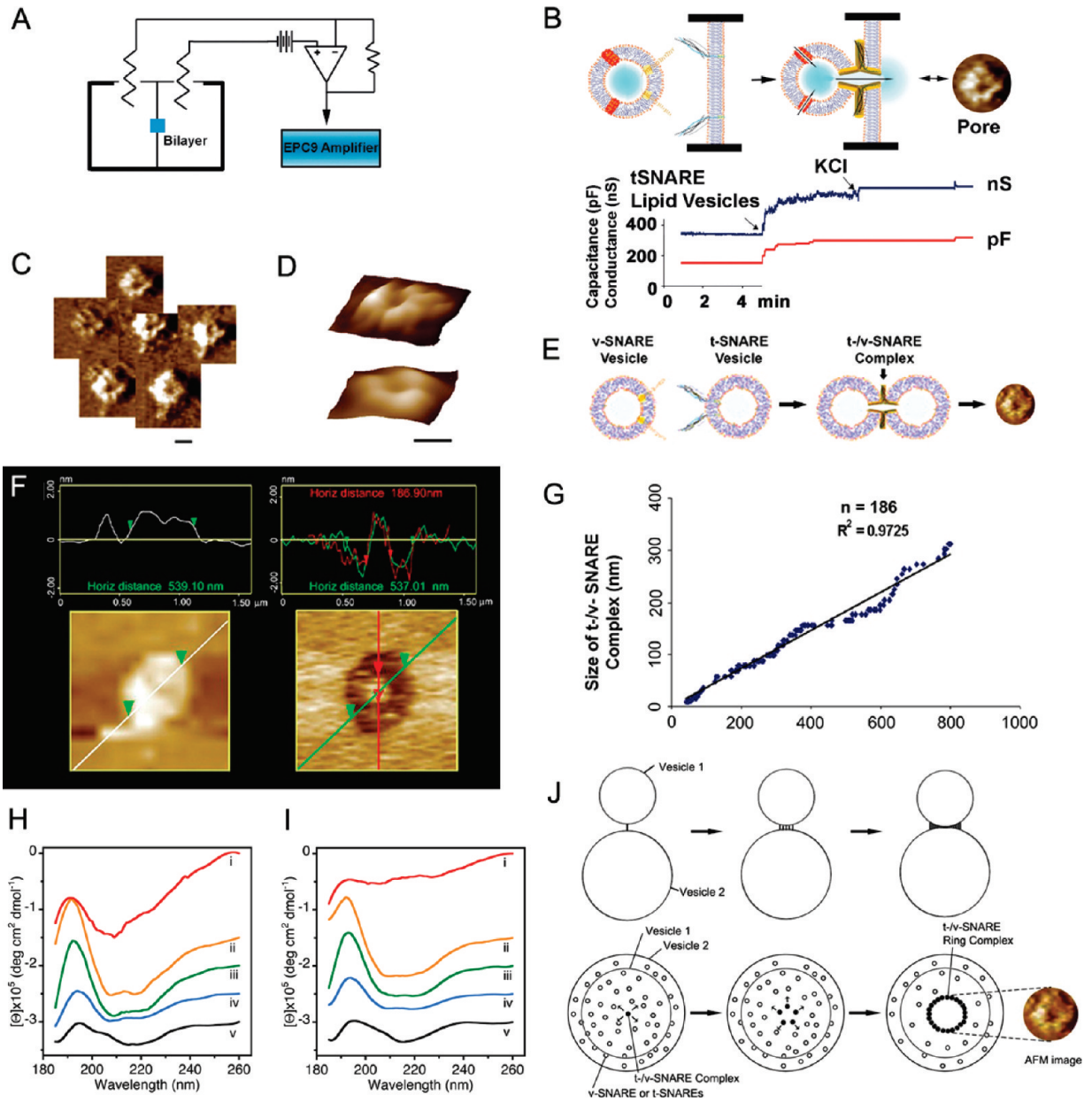

FIGURE 3: Membrane-directed assembly and disassembly of SNAREs. Opposing bilayers containing t- and v-SNAREs interact in a circular array to form conducting channels in the presence of calcium. (A) Schematic diagram of the bilayer electrophysiology setup (EPC9). (B) Lipid vesicle-containing nystatin channels (red) and a membrane bilayer with SNAREs demonstrate significant changes in capacitance and conductance. When t-SNARE vesicles were added to a v-SNARE membrane support, the SNAREs in opposing bilayers arranged in a ring pattern, forming pores as shown in the AFM micrographs. (C and D) t-/v-SNARE ring complex at low (C) and high resolution (D). The bar is 100 nm. A stepwise increase in capacitance and conductance (−60 mV holding potential) is demonstrated following docking and fusion of SNARE-reconstituted vesicles at the SNARE-reconstituted bilayer of the EPC9 electrophysiological setup (B). Docking and fusion of the vesicle at the bilayer membrane open vesicle-associated nystatin channels and cuase SNARE-induced pore formation, allowing conductance of ions from the *cis* to the *trans* side of the bilayer membrane (B). Further addition of KCl to induce gradient-driven fusion resulted in little or no further increase in conductance and capacitance, demonstrating that docked vesicles have already fused and that the membrane is intact (B). (E−G) The size of the t-/v-SNARE complex is directly proportional to the size of the SNARE-reconstituted vesicles. (E) Schematic diagram depicting the interaction of t-SNARE-reconstituted and v-SNARE-reconstituted liposomes. (F) AFM images of docked v-SNARE vesicles at a t-SNARE-reconstituted membrane, before and after it is dislodged using the AFM cantilever tip, exposing the t-/v-SNARE-ring complex at the center. (G) Note the high correlation coefficient between vesicle diameter and size of the SNARE complex. (H and I) CD data reflecting structural changes to SNAREs, both in suspension and in association with membrane. Structural changes, following the assembly and disassembly of the t-/v-SNARE complex, are shown. (H) CD spectra of purified full-length SNARE proteins in suspension and (I) in their membrane-associated state. Their assembly and NSF-ATP-induced disassembly are demonstrated: (i) v-SNARE, (ii) t-SNAREs, (iii) t-/v-SNARE complex, (iv) t-/v-SNARE with NSF, and (v) t-/v-SNARE with NSF and 2.5 mM ATP. CD spectra were recorded at 25 °C in 5 mM sodium phosphate buffer (pH 7.5), at a protein concentration of 10 μM. In each experiment, 30 scans were averaged per sample for an enhanced signal-to-noise ratio, and data were acquired on duplicate independent samples to ensure reproducibility (*45*). (J) Schematic diagram depicting the possible molecular mechanism of SNARE ring complex formation, when t-SNARE vesicles and V-SNARE vesicles meet. The process may occur due to a progressive recruitment of t-/v-SNARE pairs as the opposing vesicles are pulled toward each other, until a complete ring is established, preventing any further recruitment of t-/v-SNARE pairs to the complex. The top panel is a side view of two vesicles (one t-SNARE-reconstituted and the other v-SNARE-reconstituted) interacting to form a single t-/v-SNARE complex, leading progressively (from left to right) to the formation of the ring complex. The bottom panel is a top view of the two interacting vesicles.

AFM (*1*), reveal new cellular structures at the apical plasma membrane, in the form of "pits" and "depressions". Circular pits measuring 0.4−1.2 μm, and typically three or four depressions or pores (Figure 1A,B) measuring 100−180 nm in diameter within each pit, are found at the apical end of the cell. The basolateral membrane in acinar cells is devoid of such pit or depression structures. High-resolution AFM images of depressions in live acinar cells further reveal a cone-shaped morphology, and the depth of each cone measures 15−35 nm. Similarly, examination of resting growth hormone (GH) secretory cells of the pituitary gland (*3*), neurons, astrocytes, β-cells of the endocrine pancreas, mast cells, and chromaffin cells of the adrenal medulla (*4*, *7*, *15*, *16*) shows in each case evidence of the presence of depressions at the cell plasma membrane.

Exposure of pancreatic acinar cells to a secretagogue (mastoparan/Mast.7) results in a time-dependent increase (25−45%) in both the diameter and relative depth of depressions (Figure 2). Studies demonstrate that depressions return to their resting size on completion of cell secretion (Figure 2), with no demonstrable change in pit size (*1*, *2*). Enlargement of depression diameter and relative depth following exposure to the secretagogue correlate with secretion. Additionally, exposure of pancreatic acinar cells to cytochalasin B, a fungal toxin that inhibits actin polymerization and cell secretion, results in a 15−20% decrease in depression size and a consequent 50−60% loss of secretion (*1*). Results from these studies suggested depressions to be the fusion pores in pancreatic acinar cells. These studies further demonstrated the involvement of actin in regulation of both the structure and function of depressions. Similarly, depression in resting GH cells measuring 154 ± 4.5 nm (mean ± standard error) in diameter results in a 40% increase in depression diameter (215 ± 4.6 nm; $p < 0.01$), with no appreciable change in pit size, following stimulation of secretion (*3*). The increase in depression diameter during cell secretion and the decrease in depression diameter and loss of secretion following exposure to actin depolymerizing agents (*3*) suggested these to be secretory pores or portholes. However, the direct determination that depressions are indeed the portholes via which secretory products are released from cells finally came from immuno-AFM studies. Localization at depressions of gold-conjugated antibody to secretory proteins provided direct evidence that secretion occurs through depressions (*2*, *3*). Another example came from zymogen granules that contained the starch-digesting enzyme amylase. AFM micrographs of the localization of gold-tagged amylase-specific antibodies at depressions, following stimulation of cell secretion (*2*, *5*), demonstrated depressions to be the cells secretory portholes. Similarly, in somatotrophs of the pituitary gland, gold-tagged growth hormone-specific antibody is found to selectively localize at depressions following stimulation of secretion (*3*), and this established them as being the secretory pores or the secretory portal in these cells. Over the years, the term "fusion pore" has been loosely applied to plasma membrane dimples that originate following a secretory stimulus or to the continuity or channel established between opposing lipid bilayers during membrane fusion. Hence for clarity, the term porosome was assigned to depressions, which are permanent structures at the cell plasma membrane where secretory vesicles dock and fuse to expel intravesicular contents to the outside.

The morphology of the porosome complex facing the cytosolic compartment of the cell in exocrine pancreas (*5*), and in neurons (*4*), has also been determined at near-nanometer resolution in subcellular fractions. AFM studies on isolated plasma membrane preparations in near-physiological solution reveal scattered circular disks measuring 0.5−1 μm in diameter, with inverted cup-shaped structures (*5*). The inverted cups at the cytosolic compartment of isolated pancreatic plasma membrane preparations range in height from 10 to 15 nm. On several occasions, ZGs ranging in size from 0.4 to 1 μm in diameter were observed in association with one or more of these inverted cups, suggesting they are porosomes. To further confirm that the cup-shaped structures are porosomes, immuno-AFM studies were performed. Target membrane proteins, SNAP-23/-25 (*38*) and syntaxin (t-SNARE) (*39*), and secretory vesicle-associated membrane protein v-SNARE or VAMP (*40*) are part of the conserved protein complex involved in the fusion of opposing bilayers in the presence of calcium (*41*, *42*, *44*, *61*−*63*). If porosomes are the secretory sites for vesicle docking and fusion, then plasma membrane-associated t-SNAREs should localize at the base of the structure facing the cytosol. The t-SNARE protein SNAP-23 had previously been reported in pancreatic acinar cells (*64*). A polyclonal monospecific SNAP-23 antibody recognizing a single 23 kDa protein in immunoblots of a resolved pancreatic plasma membrane fraction demonstrated selective localization to the porosome base. These results confirmed the inverted cups in inside-out isolated pancreatic plasma membrane preparations to be porosomes, where secretory vesicles dock and fuse to release their contents during cell secretion (*5*).

The morphology of the pancreatic porosome complex has been further evaluated using transmission electron microscopy (TEM) (*6*). TEM studies confirm the porosome to possess a cup-shaped structure, with similar dimensions as determined from AFM measurement. Additionally, TEM micrographs demonstrate that pancreatic porosomes display a basketlike morphology, with three lateral and a number of vertically arranged ridges. A ring at the base of the complex is further identified (*6*) and is hypothesized to represent t-SNAREs or t-/v-SNARE complexes organized in a circular array. Studies using full-length recombinant SNARE proteins and artificial lipid membrane demonstrate that t- and v-SNAREs located in opposing bilayers interact in a circular array to form conducting channels in the presence of calcium (*44*). Earlier determination of the presence of SNAP-23 at the porosome base (*5*) suggests the circular arrangement of proteins could be t-SNAREs or the t-/v-SNARE complex. In the past decade, a number of studies have demonstrated the involvement of cytoskeletal proteins in cell secretion, some implicating their direct interaction with SNAREs (*65*−*70*). Furthermore, actin and the microtubule-based cytoskeleton have been implicated in intracellular vesicle traffic. Fodrin, which was previously implicated in exocytosis, has also been shown to directly interact with SNAREs (*68*). Studies demonstrate that α-fodrin regulates exocytosis via its interaction with the t-SNARE syntaxin family of proteins. The C-terminal region of syntaxin is known to interact with α-fodrin, a major component of the submembranous cytoskeleton. Similarly, vimentin filaments interact with SNAP23/25 and hence are able to control the availability of free SNAP23/25 for assembly of the t-/v-SNARE complex (*66*). All these findings suggest that vimentin, α-fodrin, actin, and SNAREs may be part of the porosome complex. Additional proteins such as v-SNARE, synaptophysin, and myosin may associate when the porosome establishes continuity with the secretory vesicle membrane. The globular tail domain of myosin V contains a binding site for VAMP, which is bound in a calcium-independent manner (*69*). Further interaction of myosin V with syntaxin had previously been shown to require both calcium and

calmodulin. It had also been suggested that VAMP may act as a myosin V receptor on secretory vesicles and regulate formation of the SNARE complex (*68*). Interaction of VAMP with synaptophysin and myosin V had also been reported (*69*). In agreement with these earlier findings, our studies (*4*, *5*) demonstrate the association of SNAP-23, syntaxin 2, cytoskeletal proteins actin, α-fodrin, and vimentin, and calcium channels β3 and α1c, together with the SNARE regulatory protein NSF, at the porosome complex (*4*−*6*). Additionally, chloride ion channels ClC2 and ClC3 were also identified as part of the porosome complex (*4*−*6*). Isoforms of a number of proteins identified as components of the porosome complex have also been reported using two-dimensional BAC gel electrophoresis (*6*). Three isoforms each of the calcium ion channel and vimentin have been identified in porosomes (*6*). Using yeast two-hybrid analysis, studies further confirmed the presence and interaction of some of these proteins with t-SNAREs within the porosome complex (*70*).

The size and shape of the immunoisolated porosome complex have also been determined using both negative staining EM and AFM (*6*). The morphology of immunoisolated porosomes obtained using EM and AFM is almost identical and superimposable (*6*). The immunoisolated porosome complex has also been structurally and functionally reconstituted into liposomes and bilayer membranes (*4*, *6*). Transmission electron micrographs of pancreatic porosomes reconstituted into liposomes exhibit a 150−200 nm cup-shaped basketlike morphology, similar to what is observed in its native state when co-isolated with ZGs. To test the functionality of isolated porosomes obtained from exocrine pancreas or neurons, they were reconstituted into the lipid membrane of the electrophysiological setup (EPC9) and exposed to isolated ZGs or synaptic vesicles. Electrical activity of the reconstituted membrane as well as the transport of vesicular contents from the *cis* to the *trans* compartments of the bilayer chambers was then monitored. Results from these experiments demonstrate that the lipid membrane-reconstituted porosomes are indeed functional (*4*, *6*), demonstrating isolated secretory vesicle docking, fusion, and the transfer of intravesicular contents from the *cis* to the *trans* compartment of the bilayer chamber. ZGs fuse with the porosome-reconstituted bilayer as demonstrated by an increase in capacitance and conductance, and a time-dependent transport of the ZG enzyme amylase from the *cis* to the *trans* compartment of the bilayer chamber (*6*, *8*). Amylase is detected using immunoblot analysis of the buffer in the *cis* and *trans* chambers of the bilayer apparatus (*6*, *8*). Chloride channel activity is also present in the reconstituted porosome complex, and the channel inhibitor 4,4′-diisothiocyanatostilbene-2,2′-disulfonic acid (DIDS) inhibited current activity through the porosome-reconstituted bilayer, demonstrating its requirement for porosome function. Similarly, the structure and biochemical composition of the neuronal porosome complex (Figure 1C,D), and the docking and fusion of synaptic vesicles at the structure have also been determined (*4*, *7*).

In recent years, a number of laboratories (*11*, *49*−*51*) have also demonstrated the presence of porosomes and their involvement in cell secretion from neurons, neuroendcrine cells, to acinar cells of the exocrine pancreas. Although conducted at a much lower resolution than AFM observations (*4*, *7*, *52*), recent EM studies (*49*) of the presynaptic terminal also demonstrate synaptic vesicles docked at 12−15 nm electron dense structures. Similarly in separate studies from three different laboratories using EM, AFM, and high-molecular weight dyes, on pancreatic acinar cells (*11*, *50*), and on gonadotrophs of the anterior pituitary gland (*51*), porosomes or fusion pores have been identified and implicated in cell secretion. In summary, these studies collectively demonstrate porosomes to be permanent supramolecular lipoprotein structures at the cell plasma membrane, where membrane-bound secretory vesicles transiently dock and fuse to release intravesicular contents to the outside (*8*, *9*, *16*). Porosomes in exocrine pancreas and neuroendocrine cells measure 100−180 nm, and only a 20−35% increase in porosome diameter is demonstrated following the docking and fusion of 0.2−1.2 μm diameter secretory vesicles, suggesting that secretory vesicles "transiently" dock and fuse at the base of the porosome complex to release their contents to the outside. In mammalian cells, it has long been held that secretory vesicles completely merge at the cell plasma membrane, allowing intravesicular contents to passively diffuse out of the cell during secretion. If secretory vesicles completely merge at the cell plasma membrane, the porosome structure would be totally obliterated, and the generation of partially empty vesicles following cell secretion would be inexplicable. With the discovery of the porosome and the transient docking, fusion, and dissociation of secretory vesicles at its base, the generation of partially empty vesicles following cell secretion can now be explained. In agreement, several studies from a number of laboratories report that "secretory granules are recaptured largely intact after stimulated exocytosis in cultured endocrine cells" (*53*), that "single synaptic vesicles fuse transiently and successively without loss of identity" (*54*), that "zymogen granule exocytosis is characterized by long fusion pore openings and preservation of vesicle lipid identity" (*55*), and that the "number of secretory vesicles in growth hormone cells of the pituitary remain unchanged after secretion" (*56*). It is fascinating how even single-cell organisms have developed specialized secretory structures, such as the secretion apparatus of *T. gondii* (Figure 1F) (*33*), specialized secretory systems in bacterial cells (*35*), and the trichocyst structure and its discharge and the contractile vacuole in paramecium (*34*). Therefore, it is not surprising that mammalian cells have evolved such highly specialized and sophisticated structures, the porosomes, for the precise and regulated expulsion of intravesicular contents during cell secretion, from neurotransmission (Figure 1C,D), endocrine secretion, to the secretion of digestive enzymes from the exocrine pancreas (Figure 1A,B), or the specialized porosome-like canaliculi system for secretion from human platelets (Figure 1E) (*36*, *37*).

Participation of SNAREs in Secretory Vesicle Fusion at the Porosome Base. V-SNARE and t-SNAREs need to reside in opposing membrane to appropriately interact and establish continuity across opposing bilayers (*44*). Purified recombinant t- and v-SNARE proteins, when applied to a lipid membrane, form globular complexes and do not alter membrane current. In contrast, when t-SNAREs and v-SNARE in opposing bilayers are exposed to each other in calcium buffer, they interact and are organized in a circular array, forming channel-like structures (Figure 3). These channels are conducting, since some vesicles having discharged their contents appear flat, measuring only 10−15 nm in height, compared to their height of 40−60 nm when filled. Since the t-/v-SNARE complex is established between opposing bilayers, their organization is visible only following vesicle discharge, or when vesicles are dislodged from the complex by the AFM cantilever tip (Figure 3F). Further determination of the establishment of continuity between opposing membrane via the t-/v-SNARE ring complex is demonstrated

from electrophysiological assays (Figure 3A,B). In the EPC9 electrophysiological setup (Figure 3A), the conductance and capacitance of a v-SNARE-reconstituted bilayer membrane are monitored following exposure to t-SNARE-reconstituted vesicles (Figure 3B). Nystatin, in the presence of ergosterol, forms a cation-conducting channel in lipid membranes (*57*−*60*). In calcium buffer, lipid vesicles reconstituted with t-SNAREs, nystatin, and ergosterol, when added to the *cis* compartment of the bilayer chamber, fuse with the v-SNARE-reconstituted membrane. When vesicles containing nystatin and ergosterol are incorporated into an ergosterol-free bilayer membrane of the EPC9 setup, a current spike is observed since the nystatin channel collapses as ergosterol diffuses into the lipid membrane (*57*−*60*). As a positive control, a KCl gradient tests the ability of vesicles to fuse at the lipid membrane (410 mM at *cis* and 150 mM at *trans*). The KCl gradient provides a driving force for vesicle incorporation that is independent of the influence of SNARE proteins. When t-SNARE vesicles are exposed to v-SNARE-reconstituted bilayers, vesicles fuse, which is observed as a current spike and an increase in membrane capacitance (*44*). These studies demonstrate that in the absence of a membrane, even full-length t-SNAREs and v-SNARE interact differently (*44*) and, as a result, are incapable of organizing into the physiologically relevant t-/v-SNARE ring conformation. These results called for a re-evaluation of the 2.4 Å atomic coordinates determined using X-ray crystallography on crystals of the t-/v-SNARE complex obtained from truncated and non-membrane-associated t- and v-SNARE proteins (*43*). Therefore, determination of the atomic structure of membrane-associated full-length SNAREs and their complexes remains a major challenge. At the moment, cryo-EM and electron crystallography are the most logical approaches and are being conducted in the author's laboratory.

So what is the molecular mechanism of SNARE ring complex formation, and what dictates its size? Due to the rapid formation of the t-/v-SNARE ring complex between opposing bilayers, direct observation of its formation at ultrahigh resolution has been practically impossible. Hypothetically, however, the process may involve a progressive recruitment of t-/v-SNARE pairs as the opposing vesicles are pulled toward each other, until a complete ring is established, preventing further recruitment of t-/v-SNARE pairs (Figure 3J). The size of the membrane-associated t-/v-SNARE complex, however, has been found to reflect the vesicle curvature. The larger the vesicle, the smaller its curvature and the larger the t-/v-SNARE complex (Figure 3E−G). Studies using t-SNARE-reconstituted membranes when exposed to v-SNARE-reconstituted liposomes of different sizes demonstrate that the size of the t-/v-SNARE ring complex is directly proportional to the proteoliposome size (*61*).

Disassembly of the SNARE Complex. Studies demonstrate that the soluble *N*-ethylmaleimide-sensitive factor (NSF), an ATPase, disassembles the t-/v-SNARE complex in the presence of ATP (*62*). This study was also the first confirmation by direct physical observation that NSF-ATP alone can lead to SNARE complex disassembly. Using purified recombinant NSF and t- and v-SNARE-reconstituted liposomes, the disassembly of the t-/v-SNARE complex was examined. Lipid vesicles ranging in size from 0.2 to 2 μm were reconstituted with either t-SNAREs or v-SNARE. Kinetics of association and dissociation of t-SNARE- and v-SNARE-reconstituted liposomes in solution, in the presence or absence of NSF, ATP, and AMP-PNP (the nonhydrolyzable ATP analogue), was monitored by right angle light scattering. Addition of NSF and ATP to the t/v-SNARE/vesicle mixture led to a rapid and significant increase in light scattering intensity, suggesting rapid disassembly of the SNARE complex and the consequent dissociation of vesicles (*62*). Dissociation of t-/v-SNARE vesicles occurred on a logarithmic scale that was expressed by a first-order reaction kinetics, with a rate constant k of 1.1 s^{-1}. To further determine whether NSF-induced dissociation of t- and v-SNARE vesicles is energy-driven, experiments were performed in the presence and absence of ATP and AMP-PNP. No significant change with NSF alone, or in the presence of NSF-AMP-PNP, was observed, demonstrating that t-/v-SNARE complex disassembly is an enzymatic and energy-driven process.

The role of NSF-ATP in the disassembly of the t-/v-SNARE complex has also been confirmed using an immunochemical approach. It has been demonstrated that v-SNARE and t-SNAREs formed a very stable and SDS-resistant complex (*71*). NSF binds to SNAREs and forms a stable complex when locked in the ATP-bound state (ATP-NSF). Thus, in the presence of ATP and EDTA, the VAMP antibody has been demonstrated to be able to coprecipitate the NSF-SNARE complex (*71*). Therefore, when t- and v-SNARE vesicles were mixed in the presence or absence of ATP, NSF, NSF and ATP, or NSF and AMP-PNP, followed by SDS−PAGE, and electrotransferred to nitrocellulose membrane and immunoblot analysis using syntaxin-1-specific antibody, t-/v-SNARE complex disassembly was found to be complete only in the presence of NSF-ATP. Direct observation of t-/v-SNARE complex disassembly was further assessed using AFM (*62*). When purified recombinant t-SNAREs and v-SNARE in opposing bilayers interact and self-assemble to form supramolecular ring complexes, they disassemble when exposed to recombinant NSF and ATP, as observed at nanometer resolution using AFM (*62*). Furthermore, close examination at near-nanometer resolution of NSF-ATP-induced disassembly of the SNARE complex by AFM demonstrated NSF to function as a right-handed molecular motor (*64*).

SNARE Assembly and Disassembly Assessed by Circular Dichroism Spectroscopy. Circular dichroism (CD) spectroscopy confirms the overall structure of membrane-associated SNAREs and SNARE complexes to be different from those formed in the absence of membrane (*45*). This study further confirms NSF-ATP to be sufficient for SNARE disassembly (Figure 3H,I). The overall secondary structural contents of full-length neuronal v-SNARE and t-SNAREs, and the t-/v-SNARE complex, both in suspension and membrane-associated, were determined by CD spectroscopy using an Olis DSM 17 spectrometer (*45*). CD spectroscopy reveals that v-SNARE in buffered suspension, when incorporated into liposomes, exhibits a reduced level of folding (Table 1). This loss of secondary structure following incorporation of full-length v-SNARE in membrane may result from self-association of the hydrophobic regions of the protein in the absence of a membrane. When incorporated into liposomes, v-SNARE may freely unfold without the artifactual induction of secondary structure, which is reflective of the lack of CD signals at 208 and 222 nm, distinct for α-helical content. The t-SNAREs show clearly defined peaks at both these wavelengths, consistent with a higher degree of helical secondary structures formed both in buffered suspension and in membranes, at ca. 66 and 20%, respectively (Table 1). Again, similar to v-SNARE, the membrane-associated t-SNAREs exhibit less helical content than in suspension. Similarly, there appears to be a dramatic difference in the CD signal observed in t-/v-SNARE complexes in suspension and the CD signal of those complexes

Table 1: Secondary Structural Fit Parameters of SNARE Complex Formation and Dissociation[a]

	suspension (100*f*)					membrane-associated (100*f*)				
protein[b]	α	*β*	*O*	*U*	fit[c] (nm)	α	*β*	*O*	*U*	fit[c] (nm)
v-SNARE	4	36	18	43	0.19	0	30	32	38	0.21
t-SNAREs	66	34	0	0	0.02	20	15	21	44	0.84
v-/t-SNAREs	48	52	0	0	0.02	20	19	56	5	0.38
v-/t-SNAREs with NSF	20	25	0	55	0.07	18	6	8	68	0.2
v-/t-SNAREs with NSF and ATP	3	39	18	40	0.22	1	27	34	38	0.23

[a] Abbreviations: *f*, fraction of residues in a given conformational class; α, α-helix; *β*, *β*-sheet; *O*, other (sum of turns, distorted helix, and distorted sheet); *U*, unordered. [b] Protein constructs: v-SNARE (VAMP2), t-SNAREs (SNAP-25 with syntaxin 1A), and NSF (*N*-ethylmaleimide-sensitive factor). [c] Fit represents the goodness of fit parameter expressed as the normalized spectral fit standard deviation (*11*).

that are formed when membrane-associated SNAREs interact. Interestingly, there is no increase in the level of secondary structure upon complex formation. Rather, the CD spectra of the complexes are identical to a combination of individual spectra. Moreover, membrane-associated t-/v-SNAREs are less folded than the purified SNARE complex. These data support previous AFM results which showed that lipid is required for proper arrangement of the SNARE proteins in membrane fusion. Addition of NSF to the t-/v-SNARE complex results in an increase in the unordered fraction (Table 1), which may be attributed to an overall disordered secondary structure of the NSF, and not necessarily unfolding of the t-/v-SNARE complex. In contrast, activation of NSF by the addition of ATP almost completely abolishes all α-helical content within the multiprotein complex. This direct observation of the helical unfolding of the SNARE complex using CD spectroscopy under physiologically relevant conditions (i.e., in membrane-associated SNAREs) confirms AFM reports on NSF-ATP-induced t-/v-SNARE complex disassembly (*62*). In further agreement with previously reported studies using the AFM, the consequence of addition of ATP to the t-/v-SNARE-NSF complex is disassembly, regardless of whether the t-/v-SNARE-NSF complex is membrane-associated or in buffered suspension. In earlier AFM studies, 0.16−0.2 μg/mL SNARE proteins were used, as opposed to the protein concentration of 800−1000 μg/mL required for the current CD studies. To determine if t-SNARE and v-SNARE interact differently at higher protein concentrations, both membrane-associated and in-suspension v- and t-SNARE complexes used in CD studies were imaged using AFM. In confirmation, results from the CD study demonstrated the formation of t-/v-SNARE ring complexes, only when t-SNARE liposomes are exposed to v-SNARE liposomes. Hence, higher SNARE protein concentrations are without influence on the membrane-directed self-assembly of the SNARE complex (*45*). In summary, the CD results demonstrate that v-SNAREs in suspension or when incorporated into liposomes exhibit a reduced level of folding. Similarly, t-SNAREs which exhibit clearly defined peaks at CD signals of 208 and 222 nm, consistent with a higher degree of helical secondary structure in both the soluble and liposome-associated forms, exhibit reduced levels of folding when membrane-associated. ATP-induced activation of NSF bound to the t-/v-SNARE complex results in disassembly of the SNARE complex, eliminating all α-helices within the structure. These studies are a further confirmation of earlier reports (*62*) that NSF-ATP is sufficient for the disassembly of the t-/v-SNARE complex.

SNAREs Bring Opposing Bilayers Closer, Enabling Calcium Bridging and Membrane Fusion. X-ray diffraction patterns of nonreconstituted vesicles and t- and v-SNARE-reconstituted vesicles in the absence and presence of 5 mM Ca^{2+} have been performed in the 2−4 Å diffraction range (*46*), having broad pattern spanning 2θ ranges of approximately 23−48° or *d* values of 3.9−1.9 Å with a sharp decrease in intensity on either side of the range. A broad feature of the diffractogram indicates a multitude of contacts between atoms of one vesicle as well as between different vesicles. However, two broad peaks are visible on the diffractogram, the stronger being at 3.1 Å and a weaker one at 1.9 Å, indicating that the greatest number of contacts between them have these two separating distances. The addition of Ca^{2+}, the incorporation of SNAREs at the vesicle membrane, or both influence both peaks within the 2.1−3.3 Å intensity range. The influence of Ca^{2+}, SNAREs, or both is more visible on a peak positioned at 3.1 Å in the form of an increased I_{max} of arbitrary units and 2θ. This increase in I_{max} at 3.1 Å can be explained in terms of an increased level of vesicle pairing and/or a decrease in the distance between apposed vesicles. Incorporation of t- and v-SNARE proteins at the vesicle membrane allows for tight vesicle−vesicle interaction, demonstrated again as an I_{max} shift to 30.5° or from 3.1 to 2.9 Å. Ca^{2+} and SNAREs work in a manner that induces a much greater increase in peak intensity with the appearance of shoulders at 2.8 Å.

Hydrated calcium $[Ca(H_2O)_n]^{2+}$ has more than one shell around it, and the first hydration shell around the Ca^{2+} has six water molecules in an octahedral arrangement (*37*). Calcium drives SNARE-induced fusion of opposing bilayers (*46*, *47*). SNARE interactions allow opposing bilayers to come within a distance of approximately 2.8 Å. Using light scattering and X-ray diffraction experiments involving SNARE-reconstituted liposomes, it has become clear that fusion proceeds only when Ca^{2+} ions are available between the t- and v-SNARE-apposed bilayers (*47*). Since t-SNAREs and v-SNAREs in opposing bilayers interact in a circular array to form conducting channels in the presence of calcium (*44*), it would necessitate that Ca^{2+} ions be present between the SNARE-apposed bilayers, to allow bridging of the opposing membranes. Once calcium forms such a bridge, it can no longer hold its water shells, leading to water expulsion, membrane destabilization, and fusion. To confirm results of X-ray diffraction studies and further test the hypothesis given above, atomistic molecular dynamic simulations in the isobaric−isothermal ensemble using hydrated dimethyl phosphate anions (DMP^-) and calcium cations were performed (*48*). DMP^- was chosen for the study since it represented the smallest molecular fragment of typical membrane phospholipids that retained properties of the phospholipid headgroup, while providing a significant reduction in the computational complexity and enhancing the accuracy of the study. Furthermore, the strategy of using DMP^- rather than full phospholipids in the simulation facilitates the search for spontaneously formed Ca^{2+}-phospholipid structures, which may bridge the headgroups of opposing

phospholipid bilayers. Results from the simulation study clearly demonstrated that DMP and calcium form DMP-Ca^{2+} complexes with the consequent removal of water, supporting the hypothesis. As a result of Ca^{2+}-DMP self-assembly, the distance between anionic oxygens between the two DMP molecules is reduced to 2.92 Å (*48*), which is in agreement with the 2.8 Å SNARE-induced apposition established between opposing lipid bilayers, reported from X-ray diffraction measurements (*46*). These findings provide for the first time a molecular understanding of SNARE-induced membrane fusion in cells.

CONCLUSION

In this work, the current understanding of the molecular machinery and mechanism of secretion in cells is presented. Porosomes are specialized plasma membrane structures universally present in secretory cells, from exocrine and endocrine cells to neuroendocrine cells and neurons. Since porosomes in exocrine and neuroendocrine cells measure 100−180 nm in diameter and only a 20−35% increase in porosome diameter is demonstrated following the docking and fusion of 0.2−1.2 μm diameter secretory vesicles, it is concluded that secretory vesicles "transiently" dock and fuse at the base of the porosome complex to release their contents to the outside. This is in contrast to the general belief that in mammalian cells, secretory vesicles completely merge at the cell plasma membrane, resulting in passive diffusion of vesicular contents to the cell exterior, and the consequent retrieval of excess membrane by endocytosis at a later time. Additionally, a major logistical problem with the concept of complete merging of secretory vesicle membrane at the cell plasma membrane is an explanation of the generation of partially empty vesicles following cell secretion. It is fascinating how even single-cell organisms have developed such specialized secretory machinery, like the secretion apparatus of *T. gondii*, the contractile vacuole in paramecium, and the secretory structures in bacteria. Hence, it comes as no surprise that mammalian cells have evolved such highly specialized and sophisticated structures, the porosome complex for cell secretion. The discovery of the porosome and an understanding of its structure and dynamics at nanometer resolution and in real time in live cells, its composition, and its functional reconstitution in lipid membrane have greatly advanced our understanding of cell secretion. It is evident that the secretory process in cells is a well-coordinated, highly regulated, and finely tuned biomolecular orchestra. Clearly, these findings could not have advanced without AFM, and therefore, this powerful tool has greatly contributed to a new understanding of the cell. AFM has enabled the determination of the live cellular structure−function relationship at subnanometer to angstrom resolution, in real time, contributing to the birth of the new field of nano-cell biology. Future directions will involve an understanding of the protein distribution and their arrangement at atomic resolution and a similar understanding of the structure of the t-/v-SNARE ring complex. Determination of the atomic structure of membrane-associated full-length SNAREs and their complexes, and of the neuronal porosome complex, will be accomplished using cryo-EM and electron crystallography and is currently being conducted in the author's laboratory.

ACKNOWLEDGMENT

I thank the many students and collaborators who have participated in the various studies discussed in this work.

REFERENCES

1. Schneider, S. W., Sritharan, K. C., Geibel, J. P., Oberleithner, H., and Jena, B. P. (1997) Surface dynamics in living acinar cells imaged by atomic force microscopy: Identification of plasma membrane structures involved in exocytosis. *Proc. Natl. Acad. Sci. U.S.A. 94* 316–321.
2. Cho, S.-J., Quinn, A. S., Stromer, M. H., Dash, S., Cho, J., Taatjes, D. J., and Jena, B. P. (2002) Structure and dynamics of the fusion pore in live cells. *Cell Biol. Int. 26*, 35–42.
3. Cho, S.-J., Jeftinija, K., Glavaski, A., Jeftinija, S., Jena, B. P., and Anderson, L. L. (2002) Structure and dynamics of the fusion pores in live GH-secreting cells revealed using atomic force microscopy. *Endocrinology 143*, 1144–1148.
4. Cho, W. J., Jeremic, A., Rognlien, K. T., Zhvania, M. G., Lazrishvili, I., Tamar, B., and Jena, B. P. (2004) Structure, isolation, composition and reconstitution of the neuronal fusion pore. *Cell Biol. Int. 28* 699–708.
5. Jena, B. P., Cho, S.-J., Jeremic, A., Stromer, M. H., and Abu-Hamdah, R. (2003) Structure and composition of the fusion pore. *Biophys. J. 84*, 1–7.
6. Jeremic, A., Kelly, M., Cho, S.-J., Stromer, M. H., and Jena, B. P. (2003) Reconstituted fusion pore. *Biophys. J. 85*, 2035–2043.
7. Cho, W. J., Jeremic, A., Jin, H., Ren, G., and Jena, B. P. (2007) Neuronal fusion pore assembly requires membrane cholesterol. *Cell Biol. Int. 31*, 1301–1308.
8. Jena, B. P. (2007) Secretion machinery at the cell plasma membrane. *Curr. Opin. Struct. Biol. 17*, 437–443.
9. Jena, B. P. (2005) Molecular machinery and mechanism of cell secretion. *Exp. Biol. Med. 230*, 307–319.
10. Jeremic, A. (2008) Cell secretion: An update. *J. Cell. Mol. Med. 12*, 1151–1154.
11. Paknikar, K. M., and Jeremic, A. (2007) Discovery of the cell secretion machinery. *J. Biomed. Nanotechnol. 3*, 218–222.
12. Paknikar, K. M. (2007) Landmark discoveries inintracellular transport and secretion. *J. Cell. Mol. Med. 11*, 393–397.
13. Wheatley, D. N. (2007) Pores for thought: Further landmarks in the elucidation of the mechanism of secretion. *Cell Biol. Int. 31*, 1297–1300.
14. Labhasetwar, V. (2007) A milestone in science: Discovery of the porosome—the universal secretory machinery in cells. *J. Biomed. Nanotechnol. 3*, 1.
15. Allison, D. P., and Doktyez, M. J. (2006) Cell secretion studies by force microscopy. *J. Cell. Mol. Med. 10*, 847–856.
16. Anderson, L. L. (2006) Cell secretion finally sees the light. *J. Cell. Mol. Med. 10*, 270–272.
17. Jeftinija, S. (2006) The story of cell secretion: Events leading to the discovery of the 'porosome'—the universal secretory machinery in cells. *J. Cell. Mol. Med. 10*, 273–279.
18. Leabu, M. (2006) Discovery of the molecular machinery and mechanisms of membrane fusion in cells. *J. Cell. Mol. Med. 10*, 423–427.
19. Anderson, L L. (2006) Discovery of the 'porosome': The universal secretory machinery in cells. *J. Cell. Mol. Med. 10*, 126–131.
20. Zhvania, M. G., and Lazrishvili, I. L. (2005) Discovery of a new cellular structure: Porosome. *Tsitologiia 47*, 23–27.
21. Milosacic, N., and Prodanovic, R. (2004) Porosome: A new cell structure. *Chem. Rev. 104*, 102–103.
22. Craciun, C. (2004) Elucidation of cell secretion: Pancreas led the way. *Pancreatology 4*, 487–489.
23. Singer, M. V. (2004) Legacy of a distinguished scientist: George E. Palade. *Pancreatology 3*, 518–519.
24. Zhvania, M. (2004) The discovery of the molecular mechanism of cellular secretion. *J. Biol. Phys. Chem. 4*, 43–46.
25. Wheatley, D. N. (2004) A new frontier in cell biology: Nano cell biology. *Cell Biol. Int. 28*, 1–2.
26. Anderson, L. L. (2004) Discovery of a new cellular structure—the porosome: Elucidation of the molecular mechanism of secretion. *Cell Biol. Int. 28*, 3–5.
27. Hörber, J. K. H., and Miles, M. J. (2003) Scanning probe evolution in biology. *Science 302*, 1002–1005.
28. Fernandez, J. M. (1997) Cellular and molecular mechanics by atomic force microscopy: Capturing the exocytotic fusion pore in vivo?. *Proc. Natl. Acad. Sci. U.S.A. 94*, 9–10.
29. Holden, C. (1997) Early peek at a cellular porthole. *Science 275*, 485.
30. Hoffman, M. (1997) Cell secretion: It's in the pits. *Am. Sci. 85* 123–124.
31. George, K. H. (1997) New microscope see on the nanoscale. *J. NIH Res. 9*, 32–34.
32. Dufresne, D. J. (1997) Yale team believes its AFM has imaged elusive fusion pores. *Biophotonics Int. March/April*, 30–31.

33. Joiner, K. A., and Ross, D. S. (2002) Secretory traffic in the eukaryotic parasite *Toxoplasma gondii*: Less is more. *J. Cell Biol. 157*, 557–563.
34. Hausmann, K., and Allen, R. D. (1977) Membranes and microtubules of the excretory apparatus of *Paramecium caudatum*. *Cytobiologie 15*, 303–320.
35. Kubori, T., Matsushima, Y., Nakamura, D., Uralil, J., Lara-Tejero, M., Sukhan, A., Galán, J. E., and Aizawa, S.-I. (1998) Supramolecular structure of the *Salmonella typhimurium* type III protein secretion system. *Science 280*, 602–605.
36. White, J. G. (1999) Platelet secretory process. *Blood 93*, 2422–2425.
37. White, J. G., and Clawson, C. C. (1980) The surface-connected canalicular system of blood platelets: A fenestrated membrane system. *Am. J. Pathol. 101*, 353–359.
38. Oyler, G. A., Higgins, G. A., Hart, R. A., Battenberg, E., Billingsley, M., Bloom, F. E., and Wilson, M. C. (1989) The identification of a novel synaptosomal-associated protein, SNAP-25, differentially expressed by neuronal subpopulations. *J. Cell Biol. 109*, 3039–3052.
39. Bennett, M. K., Calakos, N., and Scheller, R. H. (1992) Syntaxin: A synaptic protein implicated in docking of synaptic vesicles at presynaptic active zones. *Science 257*, 255–259.
40. Trimble, W. S., Cowan, D. W., and Scheller, R. H. (1988) VAMP-1: A synaptic vesicle-associated integral membrane protein. *Proc. Natl. Acad. Sci. U.S.A. 85*, 4538–4542.
41. Malhotra, V., Orci, L., Glick, B. S., Block, M. R., and Rothman, J. E. (1988) Role of an N-ethylmaleimide-sensitive transport component in promoting fusion of transport vesicles with cisternae of the Golgi stack. *Cell 54*, 221–227.
42. Wilson, D. W., Whiteheart, S. W., Wiedmann, M., Brunner, M., and Rothman, J. E. (1992) A multisubunit particle implicated in membrane fusion. *J. Cell Biol. 117*, 531–538.
43. Sutton, R. B., Fasshauer, D., Jahn, R., and Brunger, A. T. (1998) Crystal structure of a SNARE complex involved in synaptic exocytosis at 2.4 Å resolution. *Nature 395*, 347–353.
44. Cho, S.-J., Kelly, M., Rognlien, K. T., Cho, J., Hörber, J. K., and Jena, B. P. (2002) SNAREs in opposing bilayers interact in a circular array to form conducting pores. *Biophys. J. 83*, 2522–2527.
45. Cook, J. D., Cho, W. J., Stemmler, T. L., and Jena, B. P. (2008) Circular dichroism (CD) spectroscopy of the assembly and disassembly of SNAREs: The proteins involved in membrane fusion in cells. *Chem. Phys. Lett. 462*, 6–9.
46. Jeremic, A., Kelly, M., Cho, J., Cho, S.-J., Hörber, J. K., and Jena, B. P. (2004) Calcium drives fusion of SNARE-apposed bilayers. *Cell Biol. Int. 28*, 19–31.
47. Jeremic, A., Cho, W. J., and Jena, B. P. (2004) Membrane fusion: What may transpire at the atomic level. *J. Biol. Phys. Chem. 4*, 139–142.
48. Potoff, J. J., Issa, Z., Manke, C. W.Jr., and Jena, B. P. (2008) Ca^{2+}-Dimethylphosphate complex formation: Providing insight into Ca^{2+} mediated local dehydration and membrane fusion in cells. *Cell Biol. Int. 32*, 361–366.
49. Siksou, L., Rostaing, P., Lechaire, J.-P., Boudier, T., Ohtsuka, T., Fejtova, A., Kao, H.-T., Greengard, P., Gundelfinger, E. D., Triller, A., and Marty, S. (2007) Three-dimensional architecture of presynaptic terminal cytomatrix. *J. Neurosci. 27*, 6868–6877.
50. Larina, O., Bhat, P., Pickett, J. A., Launikonis, B. S., Shah, A., Kruger, W. A., Edwardson, M. J., and Thorn, P. (2007) Dynamic regulation of the large exocytic fusion pore in pancreatic acinar cells. *Mol. Biol. Cell 18*, 3502–3511.
51. Savigny, P., Evans, J., and McGarth, K. M. (2007) Cell membrane structures during exocytosis. *Endocrinology 148*, 3863–3874.
52. Cho, W. J., Ren, G., and Jena, B. P. (2008) EM 3D contourmaps provide protein assembly at the nanoscale within the neuronal porosome complex. *J. Microsc. 232*, 106–111.
53. Taraska, J. W., Perrais, D., Ohara-Imaizumi, M., Nagamatsu, S., and Almers, W. (2003) Secretory granules are recaptured largely intact after stimulated exocytosis in cultured endocrine cells. *Proc. Natl. Acad. Sci. U.S.A. 100*, 2070–2075.
54. Aravanis, A. M., Pyle, J. L., and Tsien, R. W. (2003) Single synaptic vesicles fusing transiently and successively without loss of identity. *Nature 423*, 643–647.
55. Thorn, P., Fogarty, K. E., and Parker, I. (2004) Zymogen granule exocytosis is characterized by long fusion pore openings and preservation of vesicle lipid identity. *Proc. Natl. Acad. Sci. U.S.A. 101*, 6774–6779.
56. Lee, J. S., Mayes, M. S., Stromer, M. H., Scanes, C. G., Jeftinija, S., and Anderson, L. L. (2004) Number of secretory vesicles in growth hormone cells of the pituitary remains unchanged after secretion. *Exp. Biol. Med. 229*, 291–302.
57. Cohen, F. S., and Niles, W. D. (1993) Reconstituting channels into planar membranes: A conceptual framework and methods for fusing vesicles to planar bilayer phospholipid membranes. *Methods Enzymol. 220*, 50–68.
58. Woodbury, D. J. (1999) Nystatin/ergosterol method for reconstituting ion channels into planar lipid bilayers. *Methods Enzymol. 294*, 319–339.
59. Kelly, M. L., and Woodbury, D. J. (1996) Ion channels from synaptic vesicle membrane fragments reconstituted into lipid bilayers. *Biophys. J. 70*, 2593–2599.
60. Woodbury, D. J., and Miller, C. (1990) Nystatin-induced liposome fusion. A versatile approach to ion channel reconstitution into planar bilayers. *Biophys. J. 58*, 833–839.
61. Cho, W. J., Jeremic, A., and Jena, B. P. (2005) Size of supramolecular SNARE complex membrane-directed self-assembly. *J. Am. Chem. Soc. 127*, 10156–10157.
62. Jeremic, A., Quinn, A. S., Cho, W. J., Taatjes, D. J., and Jena, B. P. (2006) Energy-dependent disassembly of self-assembled SNARE complex: Observation at nanometer resolution using atomic force microscopy. *J. Am. Chem. Soc. 128*, 26–27.
63. Cho, W. J., and Jena, B. P. (2007) N-Ethymaleimide sensitive factor is a right-handed molecular motor. *J. Biomed. Nanotechnol. 3*, 209–211.
64. Gaisano, H. Y., Sheu, L., Wong, P. P., Klip, A., and Trimble, W. S. (1997) SNAP-23 is located in the basolateral plasma membrane of rat pancreatic acinar cells. *FEBS Lett. 414*, 298–302.
65. Bennett, V. (1990) Spectrin-based membrane skeleton: A multipotential adaptor between plasma membrane and cytoplasm. *Physiol. Rev. 70*, 1029–1065.
66. Faigle, W., Colucci-Guyon, E., Louvard, D., Amigorena, S., and Galli, T. (2000) Vimentin filaments in fibroblasts are a reservoir for SNAP-23, a component of the membrane fusion machinery. *Mol. Biol. Cell 11*, 3485–3494.
67. Goodson, H. V., Valetti, C., and Kreis, T. E. (1997) Motors and membrane traffic. *Curr. Opin. Cell Biol. 9*, 18–28.
68. Nakano, M., Nogami, S., Sato, S., Terano, A., and Shirataki, H. (2001) Interaction of syntaxin with α-fodrin, a major component of the submembranous cytoskeleton. *Biochem. Biophys. Res. Commun. 288*, 468–475.
69. Ohyama, A., Komiya, Y., and Igarashi, M. (2001) Globular tail of myosin-V is bound to vamp/synaptobrevin. *Biochem. Biophys. Res. Commun. 280*, 988–991.
70. Cho, W. J., Jeremic, A., and Jena, B. P. (2005) Direct interaction between SNAP-23 and L-type calcium channel. *J. Cell. Mol. Med. 9*, 380–386.
71. Jeong, E.-H., Webster, P., Khuong, C. Q., Abdus Sattar, A. K., Satchi, M., and Jena, B. P. (1999) The native membrane fusion machinery in cells. *Cell Biol. Int. 22*, 657–670.
72. Bako, I., Hutter, J., and Palinkas, G. (2002) Car-Parrinello molecular dynamics simulation of the hydrated calcium ion. *J. Chem. Phys. 117*, 9838–9843.